MATERIALS CHEMISTRY
FRONTIERS

RESEARCH ARTICLE

View Article Online
View Journal | View Issue

Cite this: *Mater. Chem. Front.*, 2018, **2**, 1175

A strategy for the molecular design of aggregation-induced emission units further modified by substituents†

Zhe Peng, ‡ Yingchun Ji,‡ Zihan Huang, Bin Tong,* Jianbing Shi and Yuping Dong *

Aggregation-induced emission (AIE) molecules with strong luminescence in aggregated states have attracted persistent attention in recent years. The development of new structures of AIE units and their further modification with functional groups to satisfy more specialized applications are important research fields. However, studies on the molecular design associated with the functional modification of AIE units have not been reported to date. Herein, we designed and synthesized 13 aryl-substituted pyrrolo[3,2-*b*]pyrrole derivatives. Among these compounds, **DPP-1CN**, **DPP-1MF**, **DPP-1MF-2Me**, and **DPP-1MF-2IP** with electron-withdrawing groups on the phenyl groups at the 1,4-positions and electron-donating groups on the phenyl groups at the 2,5-positions of pyrrolo[3,2-*b*]pyrrole core showed AIE characteristics, whereas others showed aggregation-caused quenching (ACQ) characteristics. The absorption and photoluminescence (PL) emission spectra indicated that the AIE compounds exhibited weak intramolecular charge transfer (ICT) absorption and possessed large Stokes shifts, whereas the ACQ derivatives showed obvious ICT absorption. Density functional theory (DFT) calculation results suggested that the HOMOs and LUMOs of the four AIE compounds were spatially isolated that weakened the twisted intramolecular charge transfer (TICT) effect and minimized fluorescence reabsorption in the aggregated states. Single-crystal analysis also confirmed that AIE properties could be realized by the suppression of both the TICT effect and the close π···π interactions in the aggregated state. These results are beneficial for understanding the relationship between molecular structure and AIE properties. The resulting structural information provides the basis for the future rationalization of functional modification of the AIE materials.

Received 8th March 2018,
Accepted 9th April 2018

DOI: 10.1039/c8qm00096d

rsc.li/frontiers-materials

Introduction

The aggregation-induced emission (AIE) phenomenon has attracted significant attention since the first AIE molecule was reported by the Tang's group.[1] These AIE molecules overcome the defect of non-luminescence or weak emission in traditional aggregation-caused quenching (ACQ) materials in aggregated states, which are especially appealing and practically applied in optoelectronic devices,[2] luminescent sensors,[3] biomedical imaging,[4] and smart materials.[5] These applications benefit from the molecular design and the exploration of novel AIE units, in particular those with controllable structures and properties.[6]

Many building blocks, such as hexaphenylsilole,[7] tetraphenylethene (TPE),[8] distyrylanthracene,[9] and aryl-substituted pyrrole,[10] of AIE luminogens (AIEgens) have been broadly explored and systematically studied. To date, the primarily accepted AIE mechanism is based on the restriction of intramolecular motion (RIM) including the restriction of intramolecular rotations and intramolecular vibrations.[11] Despite promising early AIE units, the design and preparation of new AIEgens remained a big challenge. Moreover, two general approaches were adopted to achieve AIEgens: (i) the development of new AIE moieties such as BODIPY compounds,[12] Schiff bases,[13] and excited-state intramolecular proton transfer compounds[14] and (ii) the conversion of ACQ luminophores (ACQphores) to AIEgens. Incorporation of an AIE archetype into an ACQphore-core is an alternative synthetic methodology for converting ACQphores to AIEgens.[15]

Recently, researchers also modified ACQphores with AIE-inactive functional groups (aldehyde or alkyl group) to simply

Beijing Key Laboratory of Construction Tailorable Advanced Functional Materials and Green Applications, College of Materials Science and Engineering, Beijing Institute of Technology, 5 South Zhongguancun Street, Beijing, 100081, China. E-mail: tongbin@bit.edu.cn, chdongyp@bit.edu.cn; Tel: +86-10-6891-7390

† Electronic supplementary information (ESI) available. CCDC 1544597–1544605. For ESI and crystallographic data in CIF or other electronic format see DOI: 10.1039/c8qm00096d

‡ Zhe Peng and Yingchun Ji contributed equally to this work.

achieve AIEgens. Konishi *et al.*[16] reported that highly twisted *N*,*N*-dialkylamines and dipiperidyls were introduced into anthracene or naphthalene at the para position as AIEgens by prohibiting non-adiabatic transition and internal conversion. Li *et al.*[17] reported the ACQ-to-AIE conversion by changing the flexible chains without disturbing the original π system of naphthalene diimide derivatives. Wong *et al.*[18] demonstrated that terthiophene could present AIE characteristics upon the introduction of terminal aldehyde groups. Our previous study[19] showed that aldehyde-decorated anthracene performed ACQ-to-AIE conversion because of steric effects and intermolecular H-bonding interactions of the aldehyde groups. However, systematic investigation of the AIE behaviors by structural modification with different substituents is rarely reported.[20]

Pyrrole is an important five-membered nitrogen-containing heterocycle with a six π-electron aromatic system. Because of the abundant electron density and high aromaticity, it is a popular building block and shows widespread application in dye-sensitized solar cells[21] and second-order nonlinear optical materials.[22] Pyrrole is also used to build luminescent materials for chemical[23] and biological[24] sensors on the basis of facile structural modification. Aryl-substituted pyrrole derivatives initially developed by our group showed satisfactory results in chemical sensing, ion detection, and bioimaging.[10]

From the past research efforts, we have learned that enlargement of the conjugation and coplanarity of the pyrrole core to a pyrrolo[3,2-*b*]pyrrole core also leads to the formation of good candidates for AIEgens. Our previous results also indicated that aryl-substituted pyrrolo[3,2-*b*]pyrrole derivatives showed obvious AIE characteristics with versatile properties and applications such as in chloroform detection, polymorphism, acid response, and temperature monitoring.[25] However, there is absence of systematic investigation of the effects of categories and positions of the substituents on the AIE characteristics. Herein, we designed and synthesized a series of aryl-substituted pyrrolo[3,2-*b*]pyrrole-based derivatives with different electron-withdrawing or electron-donating substituents at different positions. The photoluminescence (PL) properties of these compounds were characterized, and then, the AIE natures of these compounds were clarified by theoretical calculations and single-crystal analysis. These results could be beneficial for providing a strategy for the molecular design of AIE building blocks for future functional modification to satisfy more specialized applications.

Results and discussion

The synthetic routes and molecular structures of the 13 compounds are illustrated in Scheme 1. All compounds were purified by silica gel column chromatography, and their structures were verified by ^{1}H and ^{13}C NMR spectroscopies and MALDI-TOF-MS analysis (^{13}C NMR of **DPP-2CN** and **DPP-12CN** were undesirable due to poor solubility at high concentrations). **DPP-2CN** and **DPP-12CN** were moderately soluble in $CHCl_3$ and THF, whereas the other 11 compounds showed good solubility in both $CHCl_3$ and THF, but poor solubility in H_2O and hexane. All compounds, except **DPP-2MF**, **DPP-2IP**, **DPP-1MF-2Me**, and **DPP-1CN-2MF**, could be crystallized *via* slow evaporation of DMF–hexane or $CHCl_3$–hexane mixtures under ambient conditions. These four compounds failed to produce good quality crystals and discernable X-ray diffraction. The detailed synthesis and characterization of the 13 compounds are described in the ESI† (S2).

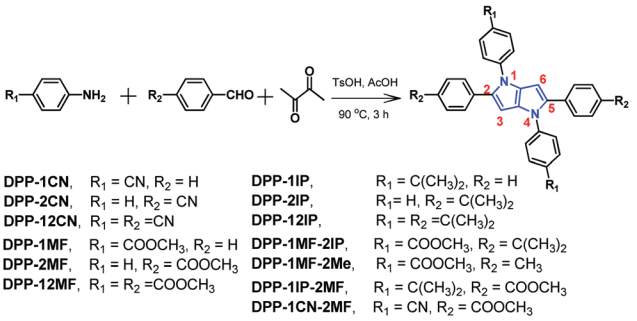

Scheme 1 The synthetic routes and molecular structures of the 13 aryl-substituted pyrrolo[3,2-*b*]pyrrole-based derivatives.

Photophysical properties

The optical properties of these compounds were studied by UV-vis absorption and PL emission spectroscopy. Their normalized absorption spectra in THF solutions (10^{-5} M) are shown in Fig. 1a. Their basic spectroscopic parameters are summarized in Table S1 (ESI†).

As shown in Fig. 1, three classes of absorption bands were observed between 320 and 410 nm with the molar extinction coefficients of 21 000–85 000 M^{-1} cm^{-1}. **DPP-1CN**, **DPP-1MF**, **DPP-1MF-2Me**, and **DPP-1MF-2IP**, with the pyrrolo[3,2-*b*]pyrrole core as the donor and the cyan groups or ester groups as acceptors, showed almost similar absorption bands with peaks/shoulder peaks at 321/362, 322/359, 322/363, and 323/363 nm, respectively. The short wavelength bands were attributed to π–π* transitions, and the shoulder peaks should be attributed to intramolecular charge transfer (ICT) transition between the cyan/ester groups and the pyrrolo[3,2-*b*]pyrrole core.[26] The redder shoulder bands were weaker than the π–π* absorption bands due to the significantly twisted structures (illustrated in the following single-crystal analysis). Both **DPP-1MF-2IP** and **DPP-1MF-2Me** showed almost the same absorption spectra as **DPP-1MF**; this indicated that electron-donating groups (EDGs) on the phenyl groups at 2,5-positions contributed negligibly to UV-vis absorption when the electron-withdrawing groups (EWGs) were located on the phenyl groups at the 1,4-positions of the pyrrolo[3,2-*b*]pyrrole core.

DPP-1IP, **DPP-2IP**, and **DPP-12IP** with isopropyl as EDGs on phenyl groups at the 1,4/2,5/1,2,4,5-positions of the pyrrolo[3,2-*b*]-pyrrole core, respectively, exhibited intense absorptions around 350 nm, which were attributed to the π–π* transition of the pyrrolo[3,2-*b*]pyrrole backbone. The UV-vis absorption bands of **DPP-1IP**, **DPP-2IP**, and **DPP-12IP** were quite similar to those reported for 1,2,4,5-tetraphenyl-1,4-dihydropyrrolo[3,2-*b*]pyrrole[25a] due to the absence of ICT. This result suggested that the

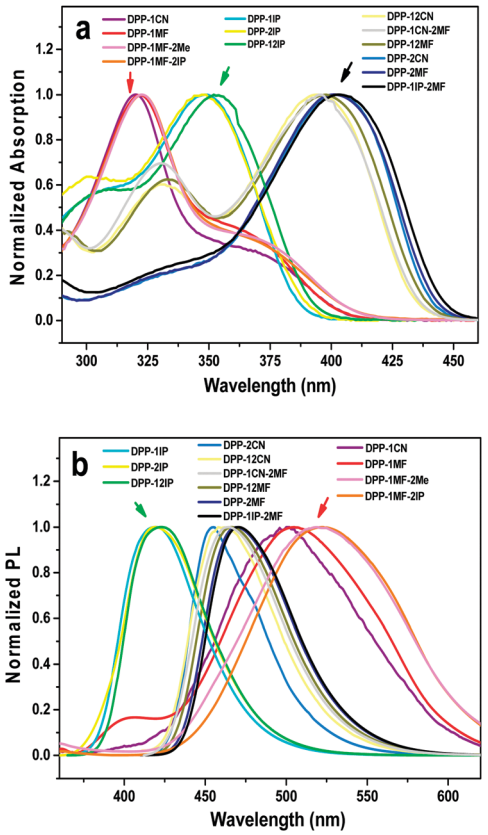

Fig. 1 The normalized absorption (a) and emission (b) spectra of 13 aryl-substituted pyrrolo[3,2-*b*]pyrrole-based derivatives in THF (10^{-5} M, excitation wavelength (λ_{ex}): 320 nm for **DPP-1CN**, **DPP-1MF**, **DPP-1MF-2Me**, and **DPP-1MF-2IP**; 350 nm for **DPP-1IP**, **DPP-2IP**, and **DPP-12IP**; and 400 nm for **DPP-12CN**, **DPP-1CN-2MF**, **DPP-12MF**, **DPP-2CN**, **DPP-2MF**, and **DPP-1IP-2MF**).

electron-donating substituents had little effect on the UV-vis absorption properties of the pyrrolo[3,2-*b*]pyrrole-based derivatives.

Moreover, three 2,5-substituted compounds, *i.e.* **DPP-2CN**, **DPP-2MF**, and **DPP-1IP-2MF**, exhibited weak absorption bands at 330 nm, which were ascribed to π–π* transitions. The strong absorption peaks at 400 nm were assigned to the distinct ICT absorption bands. Similarly, **DPP-12CN**, **DPP-12MF**, and **DPP-1CN-2MF** with quadrupole-like donor–acceptor (D–A) molecular structures showed two absorption bands at ~330 nm and ~395 nm, which were also attributed to the π–π* and ICT transitions, respectively. Since all absorption spectra of the **DPP-2MF** series are quite similar, the optical properties of the **DPP-2MF** series with different substituents were not correlated with the structural changes. All these results confirmed that the optical property of the D–A type aryl-substituted pyrrolo[3,2-*b*]-pyrrole-based derivatives could be tuned with EWGs in different positions.

The emission spectra of 13 compounds were obtained in THF (10^{-5} M), as shown in Fig. 1b. The emission spectra of the DPP series showed an emission peak at 420–520 nm with different Stokes shifts from 2900 to 11 800 cm^{-1}. The PL emission peaks of **DPP-1CN**, **DPP-1MF**, **DPP-1MF-2Me**, and **DPP-1MF-2IP** were at 500, 504, 519, and 522 nm, respectively, which exhibited the largest Stokes shifts, larger than 11 100 cm^{-1} ($\Delta\lambda$ > 180 nm). The PL emission peaks of **DPP-1IP**, **DPP-2IP**, and **DPP-12IP** were around 420 nm with minor Stokes shifts ($\Delta\lambda \approx 70$ nm). The PL emissions of **DPP-2CN**, **DPP-2MF**, **DPP-1IP-2MF**, **DPP-12CN**, **DPP-12MF**, and **DPP-1CN-2MF** peaked between 455 and 471 nm with a moderate Stokes shift ($\Delta\lambda \leq 75$ nm).

Aggregation-induced emission characteristics

As deionized water was a poor solvent for all compounds, the fluorescence spectra in THF/H_2O mixtures were obtained to investigate the fluorescence properties in the aggregated states. For **DPP-1CN**, a weak emission peak at 507 nm was observed in a dilute THF solution (Fig. 2a). In the THF/water mixture, its emission first underwent quenching with water fraction (f_w) between 10 and 60%. This phenomenon probably originated from the twisted internal charge transfer (TICT) effect,[27] which was verified by the red-shifted and decreased emission of **DPP-1CN** with an increase in solvent polarity. Then, the fluorescence intensity increased with an increase in water fraction (f_w > 60%), and ~2.2-fold emission enhancement was observed with f_w = 99% (Fig. 2b). The Tyndall effect of **DPP-1CN** in THF/water (f_w = 99%) demonstrated the formation of aggregates (inset of Fig. 2b). The quantum yields (QYs) in pure THF and in solid powder were 5.04% and 13.6%, respectively. Clearly, the

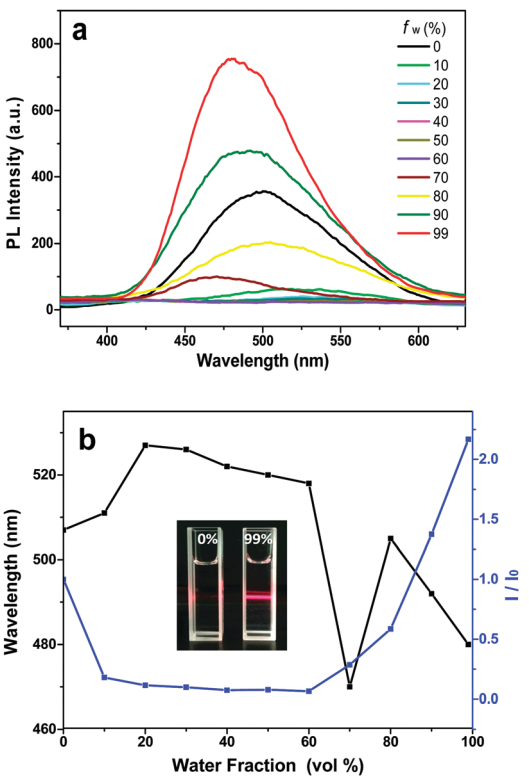

Fig. 2 (a) Fluorescence spectra of **DPP-1CN** in THF/H_2O with different water fractions. (b) A plot of wavelength and ratio of maximum fluorescence intensity of **DPP-1CN** *vs.* fraction of water (inset: the Tyndall effect of f_w = 99%). (Concentration: 10^{-5} M, λ_{ex} = 320 nm.)

PL and QY results demonstrated that **DPP-1CN** exhibited the AIE characteristic.

Interestingly, the PL emission of **DPP-1CN** with f_w = 70% was unstable. The PL intensity of this system gradually increased with increasing time and achieved 12-fold enhancement in 30 min (Fig. S1a, ESI†). This phenomenon was not monitored in other systems with different water fractions in the **DPP-1CN** solution. The particle sizes of **DPP-1CN** in 70% water at 2 and 30 min were measured by dynamic light scattering. The average particle sizes (shown in Fig. S1b and c, ESI†) were 113 nm at 2 min and 131.8 nm at 30 min, which showed that the change in PL intensity originated from variation of the aggregates formed.

The PL emission spectra of **DPP-2CN**—an isomer of **DPP-1CN**—in THF/H_2O mixtures are shown in Fig. S2a and b (ESI†). The PL emission of **DPP-2CN** remained constant at a low water content (f_w < 60%) and decreased rapidly at f_w > 70%. The ϕ_{PL} of **DPP-2CN** in the THF solution and solid powder were 95.59% and 24.7%, respectively. Both the PL emission spectra and ϕ_{PL} demonstrated that **DPP-2CN** showed a typical ACQ characteristic. A similar optical property was observed from **DPP-12CN** (Fig. S2c and d, ESI†). These results indicate that AIE/ACQ properties can be tuned by simple structural modification without changing the emissive unit.

The emission spectra of **DPP-1MF**, **DPP-1MF-2Me**, and **DPP-1MF-2IP** in THF and THF/H_2O mixtures are shown in Fig. 3a, b, and c, respectively. **DPP-1MF**, **DPP-1MF-2Me**, and **DPP-1MF-2IP** exhibited similar cyan fluorescence with maximum wavelengths at 505, 519, and 522 nm, respectively. When the water fraction increased, the emission dropped slightly. This phenomenon is typical of many fluorophores with TICT properties, where the emission is red-shifted and weakened in high polarity solvents. Dramatic increases and blue shift in emission were observed when the water fraction was over 80% for **DPP-1MF**, 70% for **DPP-1MF-2Me**, and 60% for **DPP-1MF-2IP**, indicating that all three compounds showed a typical AIE characteristic (Fig. 3d). The aggregation of **DPP-1MF**, **DPP-1MF-2Me**, and **DPP-1MF-2IP** was confirmed in a high water fraction solution, as shown in Fig. S3 (ESI†). Due to the increase in steric hindrance from **DPP-1MF**, **DPP-1MF-2Me** to **DPP-1MF-2IP**, the AIE became more obvious (Fig. 3d). The maximum PL emission of **DPP-1MF-2IP** reduced slightly at high water fractions (f_w > 80%), and the reason could be that the luminogen molecules might quickly agglomerate in a random manner to form less emissive particles. The maximal emission enhancements of **DPP-1MF**, **DPP-1MF-2Me**, and **DPP-1MF-2IP** were higher than that of **DPP-1CN**; this indicated that the methyl ester group as an EWG at the para position of the phenyl group at the 1,4-positions of the pyrrolo[3,2-*b*]pyrrole core induced a stronger AIE effect than the cyan group.

The PL spectra of **DPP-2MF**, **DPP-12MF**, **DPP-1CN-2MF**, and **DPP-1IP-2MF** in THF and THF/H_2O mixtures are obtained, as shown in Fig. S4 (ESI†). **DPP-2MF**, **DPP-12MF**, **DPP-1CN-2MF**, and **DPP-1IP-2MF** in pure THF showed strong blue-green fluorescence with maximum wavelengths at 469, 466, 464, and 470 nm, respectively. Upon continuous addition of water as a poor solvent (f_w < 60% for **DPP-2MF** and **DPP-12MF** and f_w < 70% for **DPP-1CN-2MF** and **DPP-1IP-2MF**), their PL emission intensities decreased, and emission wavelength maxima

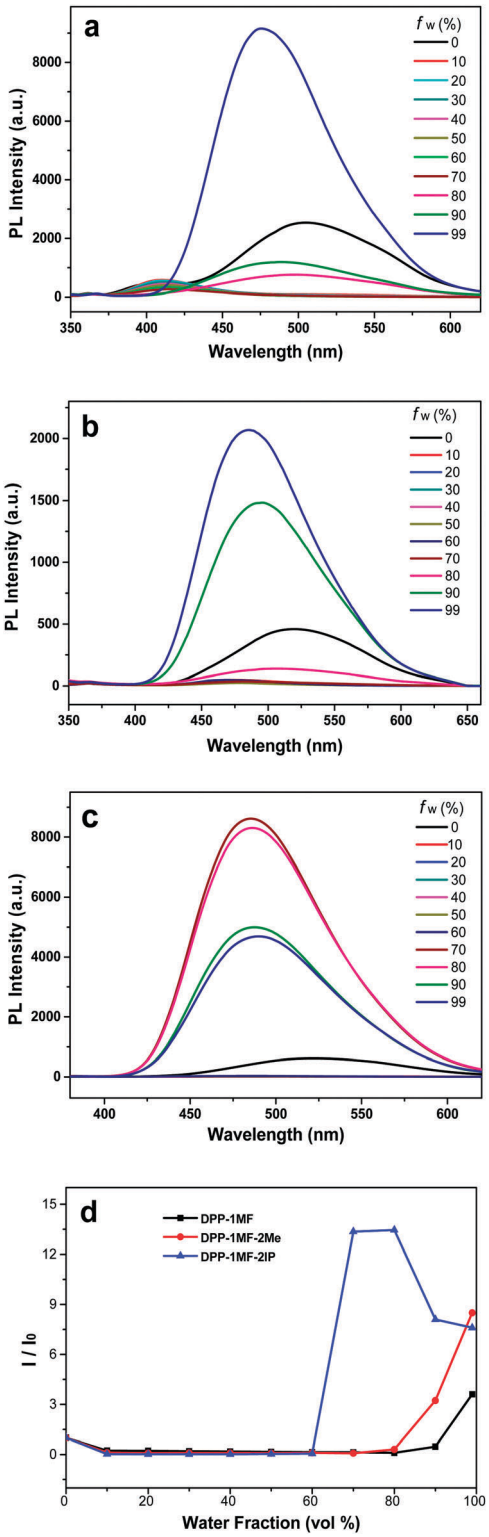

Fig. 3 Fluorescence spectra of **DPP-1MF** (a), **DPP-1MF-2Me** (b), and **DPP-1MF-2IP** (c) in THF/water with different water fractions; (d) a plot of the ratio of maximum fluorescence intensity of **DPP-1MF**/**DPP-1MF-2Me**/**DPP-1MF-2IP** *vs.* fraction of water. (Concentration: 10^{-5} M, λ_{ex} = 320 nm.)

red-shifted due to the increase of mixed solvent polarity (*i.e.*, TICT nature for D–A type molecules).

Slight emission enhancements were observed when the water fractions were 60% $\leq f_w \leq$ 80% for **DPP-2MF** and **DPP-12MF** and 70% $\leq f_w \leq$ 80% for **DPP-1CN-2MF** and **DPP-1IP-2MF**, indicating that these compounds were weak AIE but predominant TICT. When f_w was over 80%, their PL were quenched and bathochromically shifted. The PL intensities in aggregated states were lower than the initial PL intensities; this showed that the ACQ effect played a dominant role in their photophysical processes.

In addition to those of EWGs as substituents, the emission spectra of pyrrolo[3,2-*b*]pyrrole-based derivatives with EDGs were obtained. As shown in Fig. S5 (ESI†), the PL intensities of **DPP-1IP**, **DPP-2IP**, and **DPP-12IP** dropped dramatically when the water fraction was higher than 60%, exhibiting typical ACQ characteristics.

From the UV and emission results, we can conclude that the AIE-active compounds **DPP-1CN**, **DPP-1MF**, **DPP-1MF-2Me**, and **DPP-1MF-2IP** show intense π–π* absorption and weak ICT transition absorption with large Stokes shifts ($\Delta\lambda > 180$ nm). Generally, Stokes shifts over 80 nm are desirable for minimizing molecular reabsorption,[28] *i.e.*, **DPP-1CN**, **DPP-1MF**, **DPP-1MF-2Me**, and **DPP-1MF-2IP** with large Stokes shift can suppress the self-absorption effect and are favorable for AIE. Moreover, reduction of the non-radiative pathway and restriction of the formation of the TICT state can enhance emission in the aggregated state.

DFT calculations

To gain a better understanding of the correlation between molecular structure and emission property of these aryl-substituted pyrrolo[3,2-*b*]pyrrole derivatives, DFT calculations were conducted using Gaussian 09 programs at the B3LYP/6-31G(d) level. DFT calculations were performed on the basis of the single-crystal structures of **DPP-1CN**, **DPP-2CN**, **DPP-12CN**, **DPP-1MF**, **DPP-12MF**, **DPP-1IP**, **DPP-12IP**, **DPP-MF-2IP**, and **DPP-1IP-2MF**, and the molecular conformations of **DPP-2MF**, **DPP-2IP**, **DPP-1MF-2Me**, and **DPP-1CN-2MF** were optimized by the abovementioned program (Fig. 4). The highest occupied molecular orbitals (HOMOs) of all the compounds were localized on the pyrrolo[3,2-*b*]pyrrole core and phenyl groups at the 2,5-positions, which had a significant influence on the electronic structures and the optical properties.[29] However, the distributions of the lowest unoccupied molecular orbitals (LUMOs) were different. The detailed discussion of the LUMOs is as follows.

First, the LUMOs of the four AIE-active compounds were mainly localized on the phenyl groups at the 1,4-position of the pyrrolo[3,2-*b*]pyrrole core (electron acceptor moiety). Their HOMOs and LUMOs were completely separated, resulting in weak ICT transition absorption bands at around 363 nm. Therefore, introduction of EWGs into phenyl groups at the 1,4-positions for the isolation of HOMO and LUMO is beneficial to the AIE property.[17]

Second, the LUMOs of **DPP-2CN**, **DPP-2MF**, and **DPP-1IP-2MF** were mainly located on the pyrrolo[3,2-*b*]pyrrole core as well as the phenyl groups at the 2,5-positions, which showed the highest overlap with the HOMOs. All these molecules showed intense ICT absorption bands at around 400 nm and exhibited ACQ effects because the electrons in the excited state could easily relax back to the ground state *via* non-radiative transition.

Third, the LUMOs of **DPP-12CN**, **DPP-12MF**, **DPP-1CN-2MF**, **DPP-1IP**, **DPP-2IP**, and **DPP-12IP** were mainly located on the pyrrolo[3,2-*b*]pyrrole core, and the four peripheral phenyl groups. Similar molecular HOMO–LUMO orbital distribution as in **DPP-12CN**, **DPP-12MF**, and **DPP-1CN-2MF** with quadrupole-like D–A molecular structures caused similar biabsorption bands at around 330 and 395 nm. **DPP-1IP**, **DPP-2IP**, and **DPP-12IP** without EWGs showed similar absorption bands.

DPP-1IP, **DPP-2IP**, and **DPP-12IP** showed high-lying HOMO and LUMO energy levels and large energy gaps (3.85–3.87 eV). The HOMO and LUMO energy levels of the other ten pyrrolo[3,2-*b*]-pyrrole-based derivatives decreased upon introducing EWGs at different positions into the pyrrolo[3,2-*b*]pyrrole core. Compared with **DPP-1IP**, **DPP-1IP-2MF** showed a lower LUMO energy level, but equal HOMO energy. However, both the HOMO and LUMO

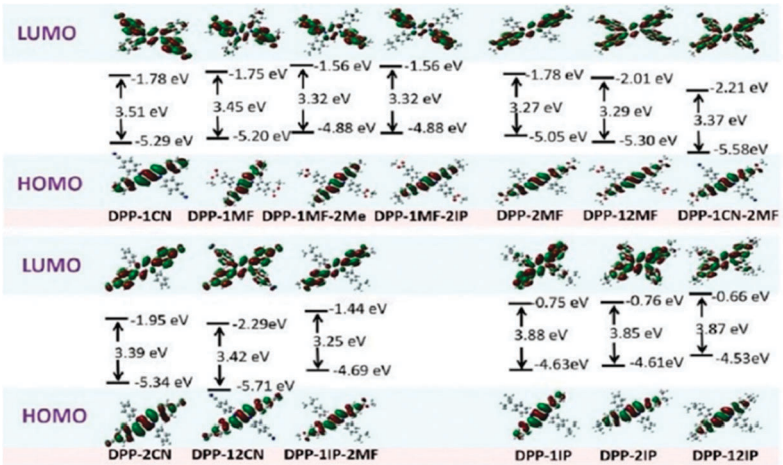

Fig. 4 Molecular orbital and energy levels of 13 aryl-substituted pyrrolo[3,2-*b*]pyrrole-based derivatives, calculated at the B3LYP/6-31G level.

energies of **DPP-1MF-2IP** were much lower than those of **DPP-2IP** due to the increase in the electron-accepting ability. Therefore, the HOMO and LUMO energies decreased gradually (**DPP-2MF** > **DPP-1MF** > **DPP-1CN** > **DPP-2CN** > **DPP-12MF** > **DPP-1CN-2MF** > **DPP-12CN**). The energy band values of the compounds **DPP-2MF**, **DPP-1MF**, **DPP-1CN**, **DPP-2CN**, **DPP-12MF**, **DPP-1CN-2MF**, **DPP-12CN**, **DPP-1IP-2MF**, **DPP-1MF-2IP**, and **DPP-1MF-2Me** were 3.27, 3.45, 3.51, 3.39, 3.29, 3.37, 3.42, 3.25, 3.32, and 3.32 eV, respectively (Fig. 4). The experimental results were consistent with these DFT calculations for **DPP-1IP** ($\Delta E_{g\text{-cal}}$ (eV)/1240/$\lambda_{onset\,abs}$ (eV) − 3.88/3.19), **DPP-12IP** (3.87/3.17), **DPP-1CN** (3.51/3.06), **DPP-1MF** (3.45/3.05), **DPP-1MF-2IP** (3.32/3.03), **DPP-12MF** (3.29/2.83), **DPP-2MF** (3.27/2.80), and **DPP-1IP-2MF** (3.25/2.79), but not for **DPP-2IP** (3.85/3.21), **DPP-1ME-2IP** (3.32/3.00), **DPP-12CN** (3.42/2.87), **DPP-1CN-2MF** (3.37/2.84), and **DPP-2CN** (3.39/2.82).

Although the emission wavelengths of 13 pyrrolo[3,2-*b*]-pyrrole-based derivatives in pure THF solution varied from 419 to 522 nm (Fig. 1b), the energy band gaps did not exactly correlate with the wavelength of fluorescence emission in solution (Table S1, ESI†) because the HOMO and LUMO were calculated based on the ground states rather than the excited states.[30]

Single-crystal structural analysis

The single-crystal analyses of **DPP-1CN** and **DPP-2CN** are shown in Fig. 5. Both **DPP-1CN** and **DPP-2CN** showed similar symmetrical structures and propeller-shaped conformations, but their dihedral angles between the phenyl and the pyrrolo[3,2-*b*]pyrrole core, packing patterns, and intermolecular interactions were quite different.

The dihedral angle between the phenyl groups at the 1,4-position and the pyrrolo[3,2-*b*]pyrrole core (ψ_1) of **DPP-1CN** was 36.3°, which was smaller than that of **DPP-2CN**. However, the dihedral angle between phenyl groups at the 2,5-position and the pyrrolo[3,2-*b*]pyrrole core (ψ_2) of **DPP-1CN** was larger than that of **DPP-2CN** (Fig. 5a and d). Both **DPP-1CN** and **DPP-2CN** molecules showed a parallel-slipped stack. No obvious π···π interactions of **DPP-1CN** were observed. The two phenyl groups at the 2,5-positions of **DPP-2CN** showed effective π···π surface overlap with a distance of 3.492 Å, the same as the two phenyl groups at 1,4-positions with a distance of 3.464 Å. The CN···H and CH···π distances of intermolecular **DPP-1CN** are respectively 2.556 and 3.001 Å, and those of **DPP-2CN** are respectively 3.171 and 2.853 Å. Both multiple intermolecular CN···H and CH···π interactions restrict intramolecular rotation, and the lack of π···π interaction enhances the emission of **DPP-1CN** in the aggregated state. In contrast, the ACQ effect of **DPP-2CN** was caused by π···π interactions.

As shown in Fig. 5, ψ_2 of **DPP-2CN** (34.2°) was smaller than that of **DPP-1CN** (43.4°). **DPP-2CN** showed higher planarity leading to longer absorption band than that in **DPP-1CN**. A similar trend was observed in the solid emission peaks.

The single-crystal structures of **DPP-1MF** and **DPP-1MF-2IP** are presented in Fig. 6. ψ_1 and ψ_2 of **DPP-1MF** were 33.6° and 55.2°, respectively. The **DPP-1MF** molecules adopted a zigzag packing pattern along the *a* axis, which was mainly dominated by intermolecular CH···π interaction with a distance of 3.256 Å. The distance between adjacent pyrrolo[3,2-*b*]pyrrole cores was 4.230 Å, indicating the lack of intermolecular π···π interactions. In addition, intermolecular CH···π interactions were observed with distances of 2.898 and 2.957 Å, and the distances of C═O···H interactions were 2.709, 2.840, and 2.912 Å. The four different dihedral angles between peripheral phenyl groups and the central pyrrolo[3,2-*b*]pyrrole core of **DPP-1MF-2IP** were different, which should be ascribed to the steric hindrance of isopropyl on phenyl groups at the 2,5-positions. The planes of the pyrrolo[3,2-*b*]pyrrole core in **DPP-1MF-2IP** were aligned parallel to the interplane distances of 4.408 and 4.049 Å along the b axis in the crystal. Multiple intermolecular CH···π interactions were observed in **DPP-1MF-2IP** with distances of 3.093, 3.152, and 3.353 Å, and the distances of C═O···H interactions were 2.633, 3.045, 3.223, 3.378, and 3.647 Å. These interactions were helpful to lock the **DPP-1MF-2IP** molecules and restrict the rotation in the aggregated state.

These results indicated that the AIE-active **DPP-1CN**, **DPP-1MF**, and **DPP-1MF-2IP** adopted rigid molecular configurations to suppress non-radiative process and boosted emission in the condensed states. Therefore, as the amounts of intermolecular H-bonding and CH···π interactions for **DPP-1CN**, **DPP-1MF**, and

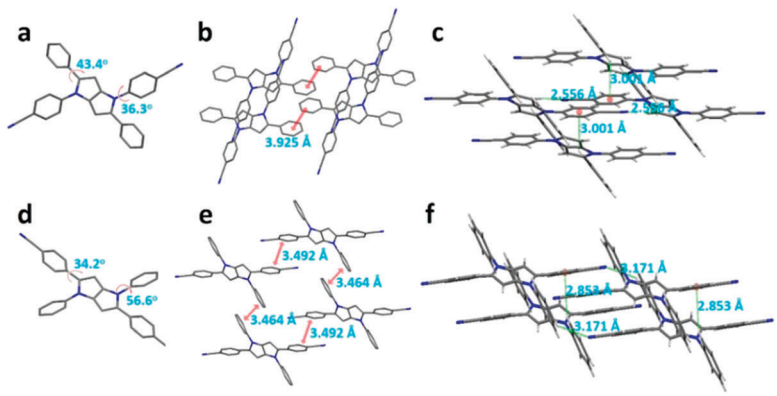

Fig. 5 The crystal structure, packing patterns, and intermolecular interactions of **DPP-1CN** (a, b, and c) and **DPP-2CN** (d, e, and f), respectively. (Hydrogen omitted for clarity (a, b, d, and e).)

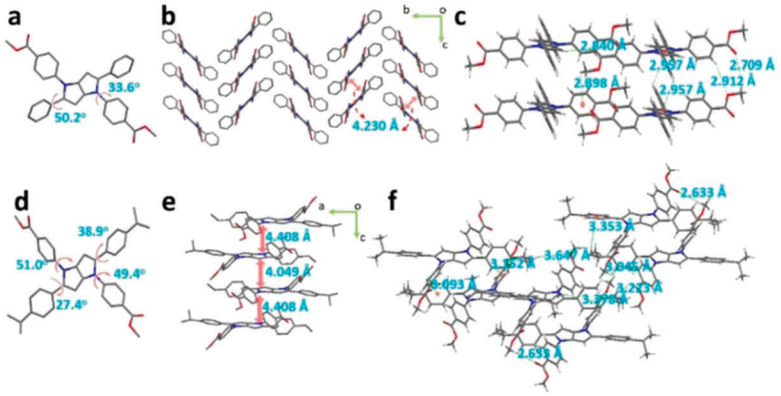

Fig. 6 The crystal structure, packing patterns, and intermolecular interactions of **DPP-1MF** (a, b, and c) and **DPP-1MF-2IP** (d, e, and f), respectively. (Hydrogen omitted for clarity (a, b, d, and e).)

DPP-1MF-2IP increased, their maximal enhancement of PL gradually increased.

It is worth noting that similarity of molecular structure can result in similar electronic structures (including HOMOs and LUMOs) among **DPP-1CN**, **DPP-1MF**, and **DPP-1MF-2IP**. For example, ψ_2 decreased from **DPP-1MF** (50.2°) to **DPP-1CN** (43.4°) to **DPP-1MF-2IP** (38.9°/27.4°). The coplanarity of the molecular structures increased accordingly. Similar trends were observed for their absorption and solid emission bands.

The single-crystal structure of **DPP-12MF** with weak AIE characteristic showed no π···π interaction. **DPP-12MF** existed in two different conformations with different dihedral angles (Fig. S6a, ESI†). The planes of two different conformational pyrrolo[3,2-*b*]pyrrole cores in **DPP-12MF** were severally aligned parallel with interspersed distances of 8.852 and 8.944 Å in one column (Fig. S6b, ESI†). Multiple intermolecular CH···π interactions between the two different conformational molecules were also observed (Fig. S6c, ESI†), accounting for the AIE characteristic of **DPP-12MF**. However, the molecule eventually showed ACQ characteristic due to the dominant ICT effect.

The single-crystal structures of the ACQ-active molecules **DPP-12CN**, **DPP-1IP-2MF**, **DPP-1IP**, and **DPP-12IP** are presented in Fig. S7 (ESI†). **DPP-12CN** and **DPP-2CN** showed similar molecular packing. **DPP-12CN** showed π···π interaction between adjacent phenyl groups at the 2,5-position with a distance of 2.748 Å.

The ψ_2 of **DPP-1IP-2MF** showed a low dihedral angle in all nine crystalline compounds with the angle of 23.7° indicating excellent planarity in the lateral molecular configuration. This high planarity also led to strong π···π interactions between adjacent phenyl groups at the 2,5-positions with a distance of 2.464 Å. π···π interactions were also observed in **DPP-12CN**, **DPP-1IP**, and **DPP-1IP-2MF**, which caused ACQ features in the condensed states. Interestingly, **DPP-12IP** without π···π interactions in crystal structures also show the ACQ characteristic. This was because **DPP-12IP** molecules adopted the malposed packing style with two columns along the *a* axis and distance of 7.743 Å. The distances of three adjacent molecules were 10.451 and 12.144 Å (Fig. S8, ESI†). This kind of packing style had enough spaces to allow the phenyl ring to freely rotate to consume the excited energy in the solid state.

Conclusions

In summary, a series of new propeller-like luminophores consisting of pyrrolo[3,2-*b*]pyrrole cores and peripheral rotatable phenyls with different electronic characteristic groups was synthesized. The effects of different electronic characteristic groups on the AIE/ACQ properties were investigated using UV-vis absorption spectra, PL emission spectra, DFT calculations, and analyses of single crystal structures. **DPP-1CN**, **DPP-1MF**, **DPP-1MF-2Me**, and **DPP-1MF-2IP** bearing strong EWGs on the phenyl groups at the 1,4-positions of the pyrrolo[3,2-*b*]pyrrole core showed obvious AIE characteristics. **DPP-2CN**, **DPP-12CN**, and **DPP-1IP-2MF** with strong EWGs on the phenyl groups at the 2,5-positions of the pyrrolo[3,2-*b*]pyrrole core and **DPP-1IP**, **DPP-2IP** and **DPP-12IP** with EDGs on the phenyl groups at the 1,4- or 2,5-positions of the pyrrolo[3,2-*b*]pyrrole core showed ACQ characteristics.

The absorption and PL emission spectra of the 13 compounds could be evidently divided into three groups. The AIE compounds exhibited weak ICT absorption and possessed the largest Stokes shifts, whereas the ACQ derivatives showed obvious ICT absorption. In addition, the HOMOs and LUMOs of the four AIE compounds are spatial isolated, which suppressed both the TICT effect and π···π stacking interactions in the aggregated state. These results not only are beneficial for the molecular design of the aryl-substituted pyrrolo[3,2-*b*]pyrrole, but also provide basic knowledge for further functional modification of other kinds of AIE units to obtain new AIE materials.

Conflicts of interest

There are no conflicts to declare.

Acknowledgements

We are grateful for the support provided by the National Basic Research Program of China (973 Program: 2013CB834704) and the National Natural Scientific Foundation of China (No. 51673024, 51328302, 21404010).

Notes and references

1 J. D. Luo, Z. L. Xie, J. W. Y. Lam, L. Cheng, H. Y. Chen, C. F. Qiu, H. S. Kwok, X. W. Zhan, Y. Q. Liu, D. B. Zhu and B. Z. Tang, *Chem. Commun.*, 2001, 1740–1741.

2 (*a*) J. Mei, N. L. C. Leung, R. T. K. Kwok, J. W. Y. Lam and B. Z. Tang, *Chem. Rev.*, 2015, **115**, 11718–11940; (*b*) F. Hu, G. X. Zhang, C. Zhan, W. Zhang, Y. L. Yan, Y. S. Zhao, H. B. Fu and D. Q. Zhang, *Small*, 2015, **11**, 1335–1344.

3 (*a*) X. Z. Yan, M. Wang, T. R. Cook, M. M. Zhang, M. L. Saha, Z. X. Zhou, X. P. Li, F. H. Huang and P. J. Stang, *J. Am. Chem. Soc.*, 2016, **138**, 4580–4588; (*b*) S. Samanta, U. Manna, T. Ray and G. Das, *Dalton Trans.*, 2015, **44**, 18902–18910.

4 (*a*) J. Y. Xiang, X. L. Cai, X. D. Lou, G. X. Feng, X. H. Min, W. W. Lou, B. R. He, C. C. Goh, L. G. Ng, J. Zhou, Z. J. Zhao, B. Liu and B. Z. Tang, *ACS Appl. Mater. Interfaces*, 2015, **7**, 14965–14974; (*b*) Z. F. Chang, L. M. Jing, B. Chen, M. S. Zhang, X. Cai, J. J. Liu, Y. C. Ye, X. D. Lou, Z. J. Zhao, B. Liu, J. L. Wang and B. Z. Tang, *Chem. Sci.*, 2016, **7**, 4527–4536; (*c*) Y. L. Wang, M. Chen, N. Alifu, S. W. Li, W. Qin, A. J. Qin, B. Z. Tang and J. Qian, *ACS Nano*, 2017, **11**, 10452–10461.

5 (*a*) C. Y. Y. Yu, R. T. K. Kwok, J. Mei, Y. Hong, S. Chen, J. W. Y. Lam and B. Z. Tang, *Chem. Commun.*, 2014, **50**, 8134–8136; (*b*) Y. X. Guo, S. Z. Gu, X. Feng, J. N. Wang, H. W. Li, T. Y. Han, Y. P. Dong, X. Jiang, T. D. James and B. Wang, *Chem. Sci.*, 2014, **5**, 4388–4393.

6 (*a*) Z. J. Zhao, B. R. He and B. Z. Tang, *Chem. Sci.*, 2015, **6**, 5347–5365; (*b*) J. Yang, J. Huang, Q. Q. Li and Z. Li, *J. Mater. Chem. C*, 2016, **4**, 2663–2684.

7 (*a*) G. N. Zhao, B. Tang, Y. Q. Dong, W. H. Xie and B. Z. Tang, *J. Mater. Chem. B*, 2014, **2**, 5093–5099; (*b*) S. Xue, L. M. Meng, R. S. Wen, L. Shi, J. W. Lam, Z. Y. Tang, B. S. Li and B. Z. Tang, *RSC Adv.*, 2017, **7**, 24841–24847.

8 (*a*) C. F. A. Gomez-Duran, R. R. Hu, G. X. Feng, T. Z. Li, F. Bu, M. Arseneault, B. Liu, E. Peña-Cabrera and B. Z. Tang, *ACS Appl. Mater. Interfaces*, 2015, **7**, 15168–15176; (*b*) S. Dalapati, E. Jin, M. Addicoat, T. Heine and D. L. Jiang, *J. Am. Chem. Soc.*, 2016, **138**, 5797–5800; (*c*) N. Sinha, L. Stegemann, T. T. Y. Tan, N. L. Doltsinis, C. A. Strassert and F. EkkehardtHahn, *Angew. Chem., Int. Ed.*, 2017, **56**, 2785–2789.

9 (*a*) J. T. He, B. Xu, F. P. Chen, H. J. Xia, K. P. Li, L. Ye and W. J. Tian, *J. Phys. Chem. C*, 2009, **113**, 9892–9899; (*b*) Y. J. Dong, B. Xu, J. B. Zhang, X. Tan, L. J. Wang, J. L. Chen, H. G. Lv, S. P. Wen, B. Li, L. Ye, B. Zou and W. J. Tian, *Angew. Chem., Int. Ed.*, 2012, **51**, 10782–10785; (*c*) J. L. Chen, S. Q. Ma, J. B. Zhang, B. Li, B. Xu and W. J. Tian, *ACS Photonics*, 2015, **2**, 313–318; (*d*) J. B. Zhang, S. Q. Ma, H. H. Fang, B. Xu, H. B. Sun, I. Chan and W. J. Tian, *Mater. Chem. Front.*, 2017, **1**, 1422–1429.

10 (*a*) X. Feng, B. Tong, J. B. Shen, J. B. Shi, T. Y. Han, L. Chen, J. G. Zhi, P. Lu, Y. G. Ma and Y. P. Dong, *J. Phys. Chem. B*, 2010, **114**, 16731–16736; (*b*) T. Y. Han, J. W. Y. Lam, N. Zhao, M. Gao, Z. Y. Yang, E. G. Zhao, Y. P. Dong and B. Z. Tang, *Chem. Commun.*, 2013, **49**, 4848–4850; (*c*) W. Y. Li, D. D. Chen, H. Wang, S. S. Luo, L. C. Dong, Y. H. Zhang, J. B. Shi, B. Tong and Y. P. Dong, *ACS Appl. Mater. Interfaces*, 2015, **7**, 26094–26100; (*d*) G. G. Liu, D. D. Chen, L. W. Kong, J. B. Shi, B. Tong, J. G. Zhi, X. Feng and Y. P. Dong, *Chem. Commun.*, 2015, **51**, 8555–8558.

11 J. Mei, Y. N. Hong, J. W. Y. Lam, A. J. Qin, Y. H. Tang and B. Z. Tang, *Adv. Mater.*, 2014, **26**, 5429–5479.

12 (*a*) X. Q. Wang, Q. S. Liu, F. Qi, L. Li, H. D. Yu, Z. P. Liu and W. Huang, *Dalton Trans.*, 2016, **45**, 17274–17280; (*b*) Y. Ooyama, M. Hato, T. Enoki, S. Aoyama, K. Furue, N. Tsunoji and J. Hshita, *New J. Chem.*, 2016, **40**, 7278–7281.

13 (*a*) T. Han, X. G. Gu, J. W. Y. Lam, A. C. S. Leung, R. T. K. Kwok, T. Y. Han, B. Tong, J. B. Shi, Y. P. Dong and B. Z. Tang, *J. Mater. Chem. C*, 2016, **4**, 10430–10434; (*b*) X. P. Gan, G. J. Liu, M. J. Chu, W. G. Xi, Z. L. Ren, X. L. Zhang, Y. P. Tian and H. P. Zhou, *Org. Biomol. Chem.*, 2017, **15**, 256–264; (*c*) Q. Feng, Y. Y. Li, L. L. Wang, C. Li, J. M. Wang, Y. Y. Liu, K. Li and H. W. Hou, *Chem. Commun.*, 2016, **52**, 3123–3126.

14 (*a*) S. Samanta, U. Manna and G. Das, *New J. Chem.*, 2017, **41**, 1064–1072; (*b*) P. Singh, H. Singh, R. Sharma, G. Bhargava and S. Kumar, *J. Mater. Chem. C*, 2016, **4**, 11180–11189; (*c*) P. S. Zhang, X. Z. Nie, M. Gao, F. Zeng, A. J. Qin, S. Z. Wu and B. Z. Tang, *Mater. Chem. Front.*, 2017, **1**, 838–845.

15 (*a*) Z. J. Zhao, P. Lu, J. W. Y. Lam, Z. M. Wang, C. Y. K. Chan, H. H. Y. Sung, I. D. Williams, Y. G. Ma and B. Z. Tang, *Chem. Sci.*, 2011, **2**, 672–675; (*b*) Q. L. Zhao, K. Li, S. J. Chen, A. J. Qin, D. Ding, S. Zhang, Y. Liu, B. Liu, J. Z. Sun and B. Z. Tang, *J. Mater. Chem.*, 2012, **22**, 15128–15135.

16 (*a*) S. Sasaki, S. Suzuki, W. M. C. Sameera, K. Igawa, K. Morokuma and G.-i. Konishi, *J. Am. Chem. Soc.*, 2016, **138**, 8194–8206; (*b*) S. Sasaki, K. Igawa and G.-i. Konishi, *J. Mater. Chem. C*, 2015, **3**, 5940–5950.

17 L. Y. Zong, Y. J. Xie, C. Wang, J. R. Li, Q. Q. Li and Z. Li, *Chem. Commun.*, 2016, **52**, 11496–11499.

18 J. Cheng, X. Z. Liang, Y. X. Cao, K. P. Guo and W. Y. Wong, *Tetrahedron*, 2015, **71**, 5634–5639.

19 Z. Peng, Z. Wang, B. Tong, Y. C. Ji, J. B. Shi, J. G. Zhi and Y. P. Dong, *Chin. J. Chem.*, 2016, **34**, 1071–1075.

20 B. Chen, H. Zhang, W. W. Luo, H. Nie, R. R. Hu, A. J. Qin, Z. Zhao and B. Z. Tang, *J. Mater. Chem. C*, 2017, **5**, 960–968.

21 (*a*) Q. Q. Li, J. Shi, H. Y. Li, S. Li, C. Zhong, F. L. Guo, M. Peng, J. L. Hua, J. G. Qin and Z. Li, *J. Mater. Chem.*, 2012, **22**, 6689–6696; (*b*) H. Y. Li, Y. Q. Hou, Y. Z. Yang, R. L. Tang, J. N. Chen, H. Wang, H. W. Han, T. Y. Peng, Q. Q. Li and Z. Li, *ACS Appl. Mater. Interfaces*, 2013, **5**, 12469–12477.

22 Q. Q. Li, C. G. Lu, J. Zhu, E. Q. Fu, C. Zhong, S. Y. Li, Y. P. Cui, J. G. Qin and Z. Li, *J. Phys. Chem. B*, 2008, **112**, 4545–4551.

23 (*a*) Y. D. Hang, J. Wang, T. Jiang, N. N. Lu and J. L. Hua, *Anal. Chem.*, 2016, **88**, 1696–1703; (*b*) Y. B. Ding, X. Li, T. Li, W. H. Zhu and Y. S. Xie, *J. Org. Chem.*, 2013, **78**, 5328–5338.

24 (*a*) L. W. He, W. Y. Lin, Q. Y. Xu and H. P. Wei, *ACS Appl. Mater. Interfaces*, 2014, **6**, 22326–22333; (*b*) Y. Li, Y. H. Zhang, H. J. Niu, C. Wang, C. L. Qin, X. D. Bai and W. Wang, *New J. Chem.*, 2016, **40**, 5245–5254.

25 (*a*) Z. Peng, X. Feng, B. Tong, D. D. Chen, J. B. Shi, J. G. Zhi and Y. P. Dong, *Sens. Actuators, B*, 2016, **232**, 264–268;

(*b*) Z. Peng, Y. C. Ji, Z. Wang, B. Tong, J. B. Shi and Y. P. Dong, *Acta Chim. Sin.*, 2016, **74**, 942–948; (*c*) Y. C. Ji, Z. Peng, B. Tong, J. B. Shi, J. G. Zhi and Y. P. Dong, *Dyes Pigm.*, 2017, **139**, 664–671.

26 Y. L. Lin, G. Chen, L. F. Zhao, W. Z. Yuan, Y. M. Zhang and B. Z. Tang, *J. Mater. Chem. C*, 2015, **3**, 112–120.

27 J. F. Araneda, W. E. Piers, B. Heyne, M. Parvez and R. McDonald, *Angew. Chem., Int. Ed.*, 2011, **50**, 12214–12217.

28 (*a*) H. Qian, M. E. Cousins, E. H. Horak, A. Wakefield, M. D. Liptak and I. Aprahamian, *Nat. Chem.*, 2016, **9**, 83–87; (*b*) H. G. Lu, Y. D. Zheng, X. W. Zhao, L. J. Wang, S. Q. Ma, X. Q. Han, B. Xu, W. J. Tian and H. Gao, *Angew. Chem., Int. Ed.*, 2016, **55**, 155–159.

29 (*a*) T. Zhang, Y. Q. Jiang, Y. L. Niu, D. Wang, Q. Peng and Z. G. Shuai, *J. Phys. Chem. A*, 2014, **118**, 9094–9104; (*b*) H. Nie, B. Chen, C. Y. Quan, J. Zhou, H. Y. Qiu, R. R. Hu, S. J. Su, A. J. Qin, Z. J. Zhao and B. Z. Tang, *Chem. – Eur. J.*, 2015, **21**, 8137–8147.

30 Y. L. Zhang, J. Li, B. Z. Tang and K. S. Wong, *J. Phys. Chem. C*, 2014, **118**, 26981–26986.